

# Phonon-Dressed Third-Harmonic Generation in Diamond

Jiaoyang Zheng,<sup>1</sup> Guru Khalsa,<sup>2</sup> and Jeffrey Moses<sup>1</sup>

<sup>1</sup>*School of Applied and Engineering Physics, Cornell University, Ithaca, NY 14853, USA*

<sup>2</sup>*Department of Materials Science and Engineering, Cornell University, Ithaca, NY 14853, USA*

(Dated: September 4, 2023)

We demonstrate a strong, elastic, frequency-upshifting optical polarizability that accompanies sum-frequency driving of Raman phonons and two-photon absorption, extending the duality of structural and optical property modification recently observed in light-driven phononics. The effect, phonon-dressed third-harmonic generation (THG), is a degenerate low-frequency analog of coherent anti-Stokes Raman scattering. In diamond, it has a cubic electric susceptibility at least 58 times larger than purely electronic THG, with polarization and frequency dependence reflecting strong coupling to Raman phonon degrees of freedom.

The close connection between structure, symmetry, and function is a principal driver of the search for new quantum materials. Leveraging this connection, prospects for ultrafast control of quantum materials have emerged employing the direct excitation of the crystalline lattice with light. Already, striking changes to functional properties such as superconductivity, magnetism and ferroelectricity have been discovered [1]. To date, structural control has usually been imparted by the strong coupling between a light-driven infrared-active (IR-active) phonon and Raman-active phonons in the anharmonic regime. When an IR-active phonon is resonantly driven to large amplitude with light it can drive Raman-active phonons of the crystal via the anharmonic lattice potential, inducing a quasi-static structural change [2], or enabling phonon upconversion to a higher frequency in the structural response [3–5]. Another recently identified pathway for Raman-IR phonon coupling is through the nonlinear ionic displacement polarizability [6]. However, when Raman-IR coupling is weak or there are no IR-active phonons, an alternative approach must be taken. One approach, as recently demonstrated in diamond and cadmium tungstate [7–9], employs sum-frequency driving of Raman-active phonons with THz light.

Ref. [6] also found that giant changes to the optical properties of crystals can accompany the structural changes induced by light-driven IR-Raman phonon coupling, and Refs. [7–9] associated the sum-frequency THz-driving of Raman phonons with the nonlinear optical effect of two-photon absorption (TPA). These optical effects can thus be useful as a signature of the structural excitation or for nonlinear optical applications. In this Letter, we identify and demonstrate a strong optical polarizability that can accompany the THz-driven Raman phonon excitation and TPA effect observed in Refs. [7–9]. The resulting optical effect, phonon-dressed third-harmonic generation (PD-THG), is an elastic Raman scattering process of a low-frequency light field to its third harmonic involving resonant driving of a Raman phonon, which may be thought of as a low-frequency, single-laser-excitation analog of coherent anti-Stokes Raman scattering (CARS). We experimentally observe this effect in diamond, an important photonic material [10–

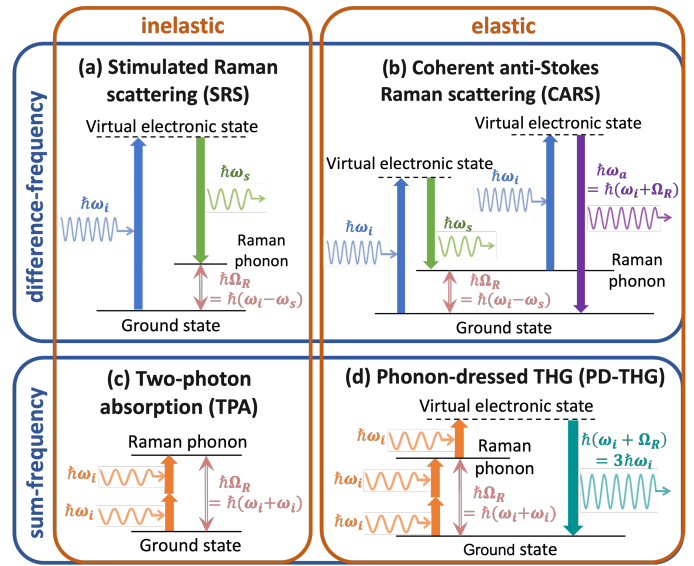


FIG. 1. Level schemes for (a) SRS and (b) its corresponding elastic process of CARS; (c) Raman-phonon excitation via the TPA pathway and (d) its corresponding elastic process of PD-THG.

14] that lacks IR-active phonons. Compared to the normal electronic pathway, this effect enhances third-harmonic generation (THG) by two orders of magnitude. We predict that it can be another order of magnitude larger with a closer match between laser and Raman linewidth than was available in our experiment, pointing to potential optical applications. The measured polarization and frequency dependence of the THG confirms the phonon-dressed mechanism and distinguishes it from the electronic pathway. Moreover, these observables provide a sensitive way not only to detect structural modes, but also to confirm the sum-frequency phonon excitation pathway. Together, these observations extend the close tie between structural and optical property modification seen in low optical frequency phonon excitation.

Normally, due to the low resonant frequency of Raman phonons (typically below 50 THz) and the relatively high frequency of lasers, Raman phonon oscillations are driven by a scattering process involving two high-frequency fields ( $\omega_i > \omega_s$ ) having a difference-frequency beat note

resonant with the Raman frequency,  $\Omega_R$ . The optically *inelastic* version of this process, stimulated Raman scattering (SRS) (Fig. 1 (a)), is most commonly associated with it. Photons are scattered from the higher to the lower (Stokes) frequency, and the residue energy is left in the system to support the lattice vibrations as an increase in phonon excited-state population. When photon momentum matching conditions are met, the elastic version of the process, coherent anti-Stokes Raman scattering (CARS) (Fig. 1 (b)), can also be efficient. This *elastic* optical four-wave mixing process produces an upshifted photon at  $\omega_i + \Omega_R$  (anti-Stokes frequency), leaving the material in its ground state. Both scattering processes involve driven coherent Raman phonon oscillations as an intermediate step (see *Supplemental Materials*).

Alternatively, for light fields below the Raman frequency, a Raman phonon can be excited via TPA [15], a process in which all optical energy is absorbed (Fig. 1(c)). Recently, Maehrlein, *et al.* demonstrated this to be a highly-efficient mechanism to excite Raman-active phonons in diamond with suppressed parasitic nonlinear effects, adding to the optical toolbox to resonantly drive infrared-forbidden lattice vibrations in solids [7]. However, this experiment did not report an accompanying optical effect that has been observed in molecular systems [16–20], THG enhancement by an intermediate resonance with a Raman vibrational mode. We expect a similar optical effect existing in crystals, linked with the Raman-active phonons, and we thus refer to it as PD-THG. In PD-THG (Fig. 1(d)), a coherence of the Raman phonon ground and excited states driven resonantly at twice the frequency of the incident photons ( $\hbar\Omega_R = 2\hbar\omega_i$ ) allows scattering from an incident photon at  $\hbar\omega_i$  to a photon of energy  $\hbar(\omega_i + \Omega_R) = 3\hbar\omega_i$ . The Raman phonon thus serves to dress an overall elastic third-order optical scattering process. PD-THG may be thought of as a low-frequency analog of the CARS effect, in which the Raman phonon coherence is established by a sum-frequency pathway rather than the usual difference-frequency pathway that is required for incident photons from typical lasers with frequencies far above the Raman resonance. Thus, as summarized in Fig 1, TPA and PD-THG are counterparts of SRS and CARS, respectively, involving driven coherent Raman phonon oscillations as an intermediate step, but driven by a sum-frequency rather than a difference-frequency beat of the incident light (see analytical details in *Supplemental Materials*).

To test for PD-THG, we used an 80- $\mu\text{m}$  thick type-IIa high-purity diamond crystal plate with [001] orientation grown by microwave plasma chemical vapor deposition (Applied Diamond, Inc.) and a specialized laser. We focus on the sole Raman-active optical phonon of diamond with  $F_{2g}$  symmetry, as investigated in Refs. [7, 9]. We measured the phonon resonant frequency ( $f_R = \Omega_R/2\pi = 39.95$  THz) and the linewidth ( $\Gamma/2\pi = 0.06$  THz) of the diamond plate with a confocal Raman microscope, and these parameters are found to be consistent with previous reports [7, 21–23] (see Figure S1 and Table S1

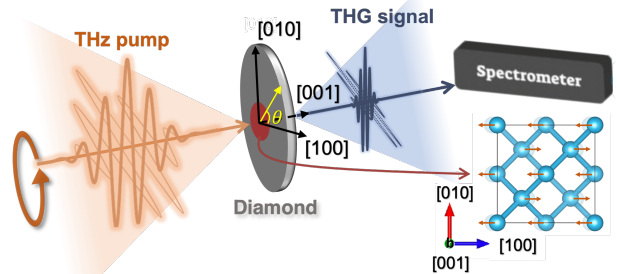


FIG. 2. Top: Simplified experiment scheme. A THz pulse directed along the [001] axis of a diamond crystal plate resonantly excites Raman-active phonons in the focusing region, producing a THG signal whose spectral intensity is then measured by a HgCdTe spectrometer. Bottom right: Schematic of the  $F_{2g}$  phonon of diamond. Orange arrows depict motion of carbon atoms (blue circles) under phonon excitation.

in *Supplemental Materials* for more details). To maximize coherent growth of the third-harmonic field, the 80- $\mu\text{m}$  plate length was chosen to equal the THG coherence length,  $L_{coh} = |\pi c/3\omega_i(n(\omega_i) - n(3\omega_i))|$ .

The PD-THG process requires an applied laser frequency at half the Raman frequency,  $\sim 20$  THz. In order to increase the likelihood of isolating the phonon-dressed effect from purely electronic THG, we wished to ensure that a large fraction of the incident laser power could resonantly excite the Raman phonon. We employed a specially designed home-built tabletop tunable THz source with a less than 0.5 THz half-width at half-maximum bandwidth, which is narrower than the FEL source in Ref. [9] and substantially narrower than the excitation pulse of Ref. [7], thus allowing a larger and significant overlap between the autoconvolution of the incident laser spectrum ( $\tilde{E}(\omega) * \tilde{E}(\omega)$ , where  $\tilde{E}(\omega)$  represents the Fourier Transform of the pump field  $E(t)$ ) and the Raman excitation band. This choice still ensured a high laser intensity at beam focus, providing  $\sim 1$ -ps pulse duration and pulse energies up to  $1.5 \mu\text{J}$  (measured by Ophir thermopile average power sensor). The THz source, described in further detail in [24], has a center frequency continuously tunable from 14 THz to 37 THz, taking advantage of a platform combining the recent technique of adiabatic difference frequency generation [25, 26] with programmable pulse-shaping to generate mid-IR pulses with customized center frequency and bandwidth.

The experimental setup is shown in Fig. 2. We used a ZnSe lens with a focal length of 15 mm to focus the THz pump onto the diamond sample, resulting in a maximum fluence of  $13 \text{ mJ/cm}^2$ . The signal emitted from the sample was collimated by another ZnSe lens and passed through two  $\text{CaF}_2$  windows to block the THz pump before passing into a HgCdTe spectrometer. Rotation of the diamond plate allowed the electric field of the linearly polarized pump to align parallel to any angle  $\theta$  in the [100]-[010] crystal plane. The THz pulse generation stage and the path of the THz beam until reaching the diamond crystal were purged by  $\text{N}_2$  gas to eliminate absorption at 20.1 THz from  $\text{CO}_2$  in the air.

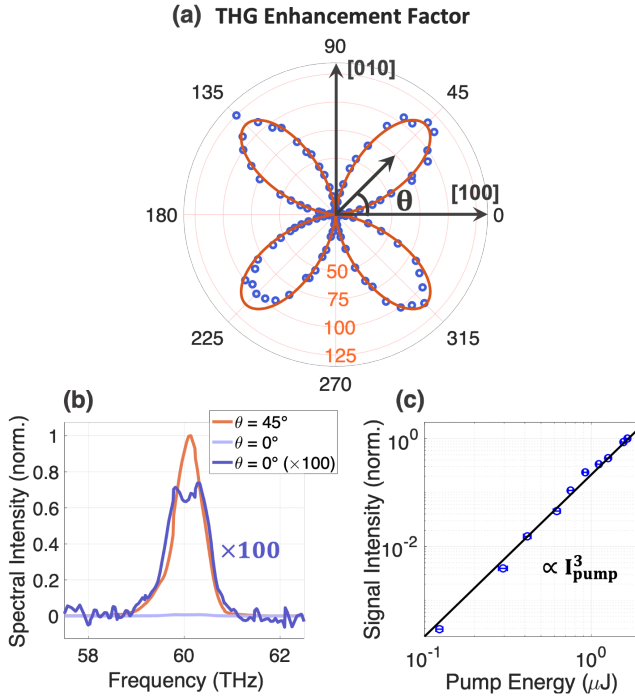


FIG. 3. (a) Polar plot of the THG power enhancement factor due to PD-THG (blue circles) vs. pump polarization direction. The orange curve is the best fit to  $\sin^2(2\theta)$ . (b) Signal spectra corresponding to  $\theta = 45^\circ$  (orange) and  $\theta = 0^\circ$  (light purple for actual signal intensity, and dark purple for intensity magnified by 100). (c) Pump energy dependence of the signal intensity measured at  $\theta = 45^\circ$ , plotted on a log-log scale, with a black line with a slope of 3 for reference.

The dependence of the THG signal power (integrated power spectrum in the vicinity of 60 THz) on light polarization angle  $\theta$  is presented in Fig. 3(a). The incident THz pump was tuned to overlap with  $f_R/2 = 19.98$  THz. The radial coordinate represents the THG enhancement factor, which is defined as the ratio of the signal power to the average of the signal power observed at the minima found at  $\theta = 0^\circ, 90^\circ, 180^\circ$ , and  $270^\circ$ . These angles are assumed to be where the pump is polarized along the [100] or [010] axis, with the [100] axis assigned arbitrarily to  $0^\circ$ . Maxima in the signal power, with THG enhancement factor over 100, are observed at  $\theta = 45^\circ, 135^\circ, 225^\circ$  and  $315^\circ$ , or when the pump is polarized along the [110] or [110] direction. Fig. 3(b) compares the signal spectra at  $\theta = 0$  and  $\theta = 45^\circ$ .

To understand the observations shown in Fig. 3, we examine the third-order electric polarization, which for low-frequency fields in diamond has two components at lowest order,

$$P^{(3)}(t) = \chi_e^{(3)} E(t) E(t) E(t) + \Pi Q_R(t) E(t), \quad (1)$$

where  $\chi_e^{(3)}$  is an approximately instantaneous non-resonant third-order electronic susceptibility originating from the anharmonic electronic potential. The second term, the origin of PD-THG, is a product of the incident electric field  $E(t)$  with the displacement of the Raman phonon  $Q_R(t)$ . This phonon can be modeled as a classi-

cal Lorentzian oscillator, with equation of motion of the mode displacement  $Q_R$  given by

$$M \left( \ddot{Q}_R + 2\Gamma \dot{Q}_R + \Omega_R^2 Q_R \right) = \Pi_{\alpha\beta} E_\alpha E_\beta, \quad (2)$$

where  $M$  is the phonon effective mass. The phonon-to-electric-field coupling originates from the dependence of the linear electronic polarization  $\chi_e^{(1)}$  on  $Q_R$ , given by the Raman polarizability tensor  $\Pi$ . For light propagating along the diamond [001] axis, this second-rank tensor has the form [21],  $\Pi = \frac{\partial \chi_e^{(1)}}{\partial Q_R} \Big|_{Q_R=0} = \Pi_0 \begin{pmatrix} 0 & 1 & 0 \\ 1 & 0 & 0 \\ 0 & 0 & 0 \end{pmatrix}$ .

Assuming the incident electric field  $E(t)$  is monochromatic light with frequency  $\omega_i$ , such that  $E(t) = E(\omega_i) e^{-i\omega_i t} + c.c.$ , and substituting it into Eqs. 1 and 2, we obtain a polarization term at the third-harmonic frequency:  $P^{(3)}(3\omega_i) = P^{(3)}(3\omega_i) e^{-i3\omega_i t} + c.c.$ , where

$$\begin{aligned} P^{(3)}(3\omega_i) &= \left[ \left( \chi_e^{(3)} + \chi_R^{(3)}(2\omega_i) \right) (E(\omega_i) \cdot E(\omega_i)) \right] \cdot E(\omega_i) \\ &\equiv P_e^{(3)} + P_R^{(3)}, \end{aligned} \quad (3)$$

in which we defined two components of  $P^{(3)}(3\omega_i)$ , the electronic-pathway contribution  $P_e^{(3)} = \chi_e^{(3)} E(\omega_i) E(\omega_i) E(\omega_i)$ , and the Raman-pathway contribution  $P_R^{(3)} = \left( \chi_R^{(3)}(2\omega_i) E(\omega_i) E(\omega_i) \right) E(\omega_i)$ . The Raman susceptibility is given by

$$\chi_R^{(3)}(2\omega_i) = \frac{\Pi_0^2}{M(\Omega_R^2 - 4\omega_i^2 - 4i\Gamma\omega_i)}. \quad (4)$$

With field polarization depending on  $\theta$  as  $\vec{E}(t) = E(t) [\cos \theta \sin \theta 0]$ , we find that the amplitude of  $Q_R$  and  $P_R^{(3)}$  are both proportional to  $\sin(2\theta)$ , as observed in Refs. [7, 22]. Consequently, the THG signal intensity, driven by the Raman pathway, is proportional to  $\sin^2(2\theta)$ . In contrast, the THG signal intensity generated from the electronic pathway ( $P_e^{(3)}$ ) exhibits near  $\theta$ -independence, as determined by the  $\chi_e^{(3)}$  tensor of diamond crystal [27] (see *Supplemental Materials* for further details). The observed signal in Fig. 3(a) demonstrates high polarization sensitivity and can be closely fitted by a  $A \sin^2(2\theta)$  function (orange curve) with maximum THG enhancement factor of  $A = 113$ . Due to experimental uncertainty in the polarization angle and purity, which means we cannot exclude some possible contribution of PD-THG at  $0^\circ$ , we conclude that the Raman-pathway contribution to the THG signal surpasses that of the purely electronic pathway by at least a factor of 113.

Fig. 3(c) summarizes a study of the THG signal intensity dependence on incident pump energy at  $\theta = 45^\circ$ . On a log-log scale, the data matches well to a line with slope of 3. This confirms a THG process as the origin of the measured signal and indicates a largely-undiminished 20-THz pump and unsaturated Raman phonon oscillation amplitude. These observations allow us to approximate that the THG enhancement observed in Fig. 3(a) is equivalent to  $|P_R^{(3)} + P_e^{(3)}|/P_e^{(3)}|^2$  and the susceptibility ratio

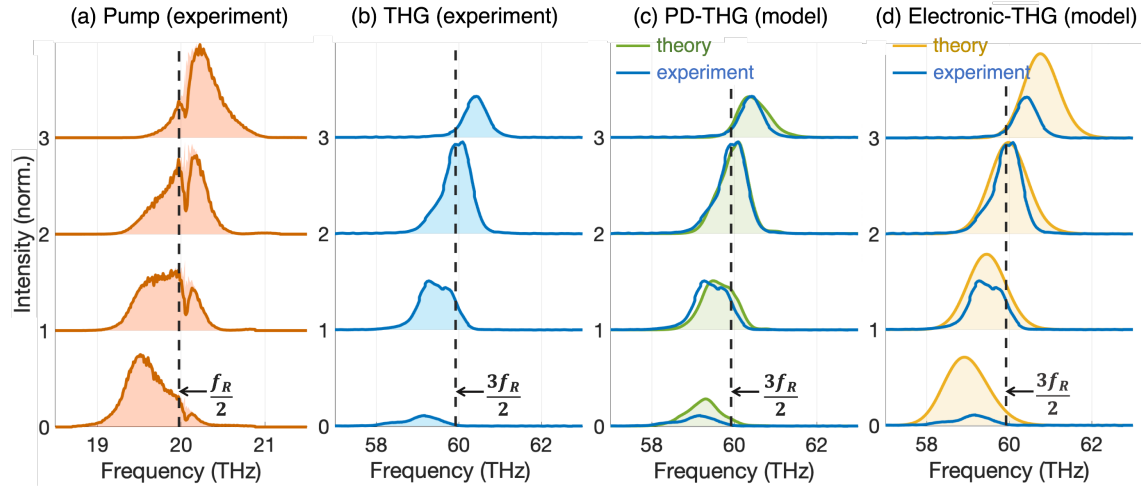


FIG. 4. Spectral intensity measurements of the (a) THz pump and (b) generated THG signal, with comparison of the measured signal (blue) to predictions of the (c) PD-THG model and (d) electronic THG model. The model predictions are normalized such that the maximum obtained from each model matches that of the experiments when closest to resonance (2<sup>nd</sup> row).

$|\chi_R^{(3)}(\Omega_R)/\chi_e^{(3)}|$  at Raman resonance is  $\geq 58$  (see *Supplemental Materials*).

As the Raman phonon oscillation and the PD-THG is predicted to have a strong frequency dependence, we tuned the pump laser to four central frequencies in the range of 19 THz to 21 THz, with spectra shown in Fig. 4(a). As expected, the corresponding measured THG signal spectra (Fig. 4 (b)) sharply increase in intensity when the pump central frequency is close to  $f_R/2$  and the signal central frequency is close to  $3f_R/2$ . To test these measurements against theory, we incorporated the pump spectra into our theoretical model (see *Supplemental Materials*), and obtained the corresponding signal spectra for each of the PD-THG mechanism (Fig. 4 (c)) and the pure electronic-THG mechanism (Fig. 4 (d)) acting alone. We note that a consistent dip in the pump spectra observed at 20.1 THz is an artefact of the measurement, resulting from CO<sub>2</sub> absorption along the measurement path into the spectrometer that was impractical to purge with N<sub>2</sub>. To correct this for use in our models, we applied a Lorentzian absorption model to compensate for the spectral dip and estimate the actual pump spectrum at the diamond crystal position (indicated by the shaded region in Fig. 4 (a)).

The PD-THG model (Fig.4 (c)) accurately captures both the experimental trend in signal intensity and spectral shape, with a discrepancy observed when the pump is furthest from resonance. In contrast, the electronic-THG model predicts a signal intensity that lacks sensitivity to the pump frequency and generally produces a broader spectrum centered further from resonance than the measurement. Both differences in the model predictions can be understood through the form of the nonlinear polarization (refer to Eq. 24 in *Supplemental Materials*), whereby PD-THG contains an implicit convolution between the Fourier transform of the frequency-dependent Raman coherence and the pump electric field,  $\tilde{Q}_R(\omega) * \tilde{E}(\omega)$ , while electronic-THG involves only a double autoconvolution of the Fourier transform of the pump

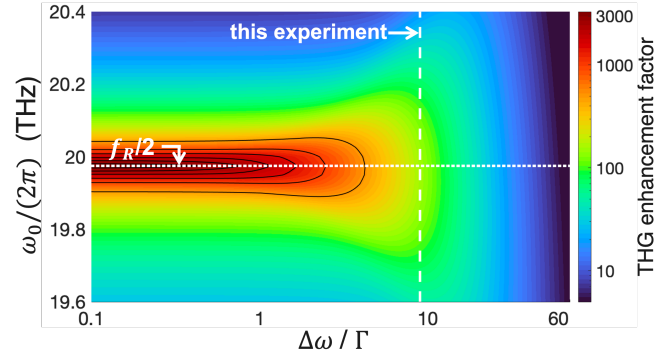


FIG. 5. PD-THG enhancement factor as a function of pump center frequency ( $\omega_0$ ) and the ratio of pump bandwidth over the Raman mode linewidth ( $\Delta\omega/\Gamma$ ). The horizontal line indicates half the Raman resonant frequency, and the vertical line represents the THz pulse bandwidth of our experiment.

electric field.

The obtained susceptibility ratio at resonance,  $|\chi_R^{(3)}(\Omega_R)/\chi_e^{(3)}| \geq 58$ , enables extrapolation of the THG enhancement factor,  $|(P_R^{(3)} + P_e^{(3)})/P_e^{(3)}|^2$ , for different combinations of pump central frequency  $\omega_0$  and bandwidth  $\Delta\omega$  (FWHM), as shown in Fig. 5. This analysis suggests a much larger enhancement is possible. The pump pulses employed in our experiment possess a bandwidth  $\sim 9$  times wider than the Raman linewidth  $\Gamma$  and result in an enhancement factor of  $\sim 100$ . However, for pump bandwidths narrower than  $\Gamma$  (corresponding to a pulse duration of  $>10$  ps), the enhancement of the THG efficiency approaches its maximum of  $|\chi_R^{(3)}(\Omega_R)/\chi_e^{(3)}|^2 \sim 3300$ , indicating the great potential of lattice vibrations to modify the optical properties of crystals. On the other hand, for shorter pump pulses of 100-fs duration, the predicted THG enhancement factor falls to  $\sim 5$ .

In this report, we demonstrate a strong frequency up-shifting nonlinear optical response of diamond crystals to low-frequency light due to Raman scattering, with nonlinear susceptibility at least 58 times larger than the ordinary response. This optical response is intimately tied

to the structural response of the material. Each response has relevance.

From a fundamental nonlinear optics perspective, our study expands upon the generalization of Raman scattering in crystals to low-frequency optical fields by demonstrating a photon scattering process analogous to CARS but via a sum-frequency excitation pathway. As such, it possesses practical advantages similar to CARS. For example, in contrast to SRS, PD-THG produces a strong optical signal at a frequency distinct from the incident light, making it simple to detect. In contrast to purely electronic THG, PD-THG has a highly sensitive dependence on light polarization direction and frequency. These characteristics suggest new applications in areas such as spectroscopy, infrared-controlled nonlinear optical switching, and orientation diagnostics. We highlight that PD-THG might be used for spectroscopic applications amenable to THz and mid-infrared light with the unprecedented feature for any non-impulsive stimulated Raman process of requiring only a single incident laser field rather than the usual two or three. We further note that the sum-frequency Raman phonon excitation pathway of PD-THG may be generalized to other, less degenerate instances of phonon-dressed four-wave mixing as a straightforward extension of our work. For example, when applying two different THz laser beams,  $E_1$  and  $E_2$ , with a sum-frequency beat note slightly detuned away from  $\Omega_R$ , there's a significant cross-phase modulation between the two beams, affecting each other's refractive index markedly. This process is analogous to the TPA in the degenerate scenario where only a single beam at  $\omega_i = \Omega_R/2$  is present. Finally, diamond has attracted considerable recent interest as a next-generation photonic material due to its excellent linear and nonlinear optical properties and relevance to quantum information science [10–14]. In virtue of its strongly enhanced frequency upconversion susceptibility, PD-THG adds ad-

ditional nonlinear optical capability to the diamond photonic platform. The phonon-dressed pathway may also allow higher-order (e.g., 5<sup>th</sup>, 7<sup>th</sup>, 9<sup>th</sup>) harmonic generation processes to become efficient, potentially allowing the incident field near 20 THz to couple to the telecom range.

From the perspective of structural excitation, our report clarifies that PD-THG and the TPA process studied previously [7, 8] are optical polarization effects – elastic and inelastic, respectively – that both accompany the coherent sum-frequency driving of Raman phonon oscillations in a crystal. PD-THG, like infrared-resonant Raman scattering [6], is thus in a category of optical polarizations that are made strong via a Raman resonance that also provides a means for structural control. This duality allows the strong optical effect to be used as a convenient marker of the concurrent structural excitation and to distinguish the sum-frequency excitation pathway, a problem previously tackled by means of two-dimensional THz spectroscopy [8]. In future work, we note that in analogy to time-domain anti-Stokes Raman scattering [9], the time-domain evolution of the coherent phonon amplitude might be resolved by applying a pump and time-delayed probe at the same incident frequency  $\omega_i = \Omega_R/2$  with a small angular separation, and following the resulting noncollinear PD-THG signal. This technique does not require carrier-envelope phase stable THz pump pulses. In conclusion, in addition to its value as a strong nonlinear optical response, PD-THG may offer a powerful laser-lab-scale diagnostic for the growing field of light-driven structural control in condensed matter physics.

This research was primarily supported through the Cornell University Materials Research Science and Engineering Center DMR-1719875. Additional support for the optical instrumentation was provided by the Kavli Institute at Cornell.

---

[1] A. S. Disa, T. F. Nova, and A. Cavalleri, *Nat. Phys.* **17**, 1087 (2021).

[2] M. Först, C. Manzoni, S. Kaiser, Y. Tomioka, Y.-n. Tokura, R. Merlin, and A. Cavalleri, *Nat. Phys.* **7**, 854 (2011).

[3] D. M. Juraschek and S. F. Maehrlein, *Phys. Rev. B* **97**, 174302 (2018).

[4] A. Melnikov, K. Boldyrev, Y. G. Selivanov, V. Martovitskii, S. Chekalin, and E. Ryabov, *Phys. Rev. B* **97**, 214304 (2018).

[5] M. Kozina, M. Fechner, P. Marsik, T. van Driel, J. M. Głownia, C. Bernhard, M. Radovic, D. Zhu, S. Bonetti, U. Staub, et al., *Nat. Phys.* **15**, 387 (2019).

[6] G. Khalsa, N. A. Benedek, and J. Moses, *Phys. Rev. X* **11**, 021067 (2021).

[7] S. Maehrlein, A. Paarmann, M. Wolf, and T. Kampfrath, *Phys. Rev. Lett.* **119**, 127402 (2017).

[8] C. L. Johnson, B. E. Knighton, and J. A. Johnson, *Phys. Rev. Lett.* **122**, 073901 (2019).

[9] O. Sato, K. Yoshida, H. Zen, K. Hachiya, T. Goto, T. Sagawa, and H. Ohgaki, *Phys. Lett. A* **384**, 126223 (2020).

[10] I. Aharonovich, A. D. Greentree, and S. Prawer, *Nat. Photonics* **5**, 397 (2011).

[11] K. Tsakmakidis, *Nat. Mater.* **12**, 596 (2013).

[12] B. Hausmann, I. Bulu, V. Venkataraman, P. Deotare, and M. Lončar, *Nat. Photonics* **8**, 369 (2014).

[13] A. Sipahigil, R. E. Evans, D. D. Sukachev, M. J. Burek, J. Borregaard, M. K. Bhaskar, C. T. Nguyen, J. L. Pacheco, H. A. Atikian, C. Meuwly, et al., *Science* **354**, 847 (2016).

[14] E. Janitz, M. K. Bhaskar, and L. Childress, *Optica* **7**, 1232 (2020).

[15] Y. Shen, *The Principles of Nonlinear Optics*, Wiley classics library (Wiley, 2003).

[16] C. She and K. W. Billman, *Appl. Phys. Lett.* **27**, 76 (1975).

[17] H. Kildal and T. Deutsch, *IEEE J. Quantum Electron.*

**12**, 429 (1976).

[18] H. Kildal and S. Brueck, *Phys. Rev. Lett.* **38**, 347 (1977).

[19] Y. Miyamoto, H. Hara, T. Hiraki, T. Masuda, N. Sasao, S. Uetake, A. Yoshimi, K. Yoshimura, and M. Yoshimura, *J. Phys. B: At. Mol. Opt. Phys.* **51**, 015401 (2017).

[20] J. F. Kinder, F. Cipura, and T. Halfmann, *Phys. Rev. A* **103**, 052808 (2021).

[21] S. Solin and Å. Ramdas, *Phys. Rev. B* **1**, 1687 (1970).

[22] K. Ishioka, M. Hase, M. Kitajima, and H. Petek, *Appl. Phys. Lett.* **89**, 231916 (2006).

[23] M. Levenson, C. Flytzanis, and N. Bloembergen, *Phys. Rev. B* **6**, 3962 (1972).

[24] W.-Z. Chang, J. Zheng, N. Flemens, D. Heberle, and J. Moses, in *Conference on Lasers and Electro-Optics* (Optica Publishing Group, 2021), p. SW3Q.5.

[25] H. Suchowski, P. R. Krogen, S.-W. Huang, F. X. Kärtner, and J. Moses, *Opt. Express* **21**, 28892 (2013).

[26] P. Krogen, H. Suchowski, H. Liang, N. Flemens, K.-H. Hong, F. X. Kärtner, and J. Moses, *Nat. Photonics* **11**, 222 (2017).

[27] M. Levenson and N. Bloembergen, *Phys. Rev. B* **10**, 4447 (1974).